

A high-cycle fatigue apparatus at 20 kHz for low-cycle fatigue/high-cycle fatigue interaction testing

T. E. MATIKAS

Greek Atomic Energy Commission, Athens, Greece

Received in final form 6 April 2001

ABSTRACT High-cycle fatigue (HCF) failures in aircraft engines are attributed to material damage states, created during processing or by in-service loading and environmental conditions, and then propagated to failure by HCF loading. The loading configuration experienced by aircraft engine turbine blades consists of an axial load caused by the centrifugal acceleration during rotation combined with the tensile and compressive loads caused by the natural vibrations of the blades themselves. To simulate these loading conditions a new testing apparatus was developed that is capable of providing interactive low-cycle fatigue/high-cycle fatigue (LCF/HCF) loading, in ratios (of magnitude and frequency) that give a realistic simulation of the actual flight loads experienced by engine components. This testing apparatus is based on a HCF cell operating at 20 kHz. The cell can also be integrated to a servo-hydraulic load frame, which provides a second fatigue cycle. The objective of this study was to demonstrate the capabilities of the new HCF apparatus via thermographic measurements and by performing LCF/HCF interaction tests.

Keywords high-cycle fatigue; titanium alloys; ultrasonic fatigue.

INTRODUCTION

The concept of high-frequency fatigue testing has been around since the 1920s, however, fatigue testing at ultrasonic frequencies was just being pioneered in the 1950s by researchers such as Mason¹ and Neppiras.² The problem of designing resonant vibrators for a variety of applications has been addressed by a number of researchers.^{3–5} Such applications of ultrasonic resonators include ultrasonic cleaning, welding, atomization of liquids, etc. Different types of transducers can be used to convert an output voltage to a mechanical vibration. Piezoelectric and magnetostrictive ultrasonic transducers have been used in various configurations to provide longitudinal,² flexural,⁶ torsional, or transverse loads. The transducer–specimen arrangement with one end of the specimen vibrating freely (known as the single transducer system) is the simplest ultrasonic fatigue set-up, but it has serious limitations as it operates at null mean load. A variation of this set-up is the double transducer

system, where the set is symmetrical about the specimen.⁷ This arrangement is much more complicated than the single transducer system because two complete sets of components are needed. It also requires that the transducers must be exactly in phase or the waves will not superimpose properly. However, the double transducer system can easily be installed into a load frame to provide either a static load⁸ or a second fatigue cycle. Drossis⁹ developed an ultrasonic fatigue apparatus and performed high-cycle fatigue (HCF) experiments superimposing a second fatigue cycle onto the HCF cycle. The extensive work of Stanzl *et al.*¹⁰ should also be mentioned—they studied fatigue crack growth at 20 kHz in various materials including aluminium alloys undergoing environmental degradation—as well as the work of Bathias *et al.*,^{11–14} who calculated the stress intensity factor for ultrasonic fatigue tests, which are displacement controlled. Finally, the chapter on ultrasonic fatigue in the ASME Handbook¹⁵ contains a nice review of the history and the various devices used in ultrasonic fatigue.

The ultrasonic fatigue apparatus presented in this article uses the single transducer concept while overcoming the limitations arising from the free vibrations of the sample allowing interaction of the HCF cycle with a

Correspondence: T. E. Matikas, Greek Atomic Energy Commission, PO Box 60092, 15310 Agia Paraskevi Attikis, Athens, Greece.
E-mail: matikas@otenet.gr

second fatigue cycle. The HCF cell is based on an ultrasonic vibrating source used to apply compressional waves to the specimen. For the specimen to resonate at ultrasonic frequencies, the specimen length must be such that a standing displacement wave is formed along its length.¹⁶ The displacement wave in turn causes a strain wave that loads the specimen. The apparatus operates at 20 kHz, although frequencies in the range of 10–40 kHz could be used for HCF testing. There are advantages for using this frequency range in ultrasonic fatigue as: (i) frequencies greater than 18 kHz are above the audible range for humans; and (ii) since the resonant length of the specimen is inversely proportional to the frequency there is a finite limit on the upper testing frequency that can be used. The 10–40 kHz range coincides with a specimen resonance length of approximately 5 to 15 cm for most metals.

The ultrasonic fatigue testing system described in this paper has the following capabilities. First, the ultrasonic fatigue frame enables, in addition to the tensile stress, compressive stresses to be applied during low-cycle fatigue (LCF), which gives the flexibility of performing interaction tests with many different *R* ratios. Second, the apparatus allows for the testing of specimens designed with a symmetric geometry. Preserving the geometrical symmetry of the sample is essential for obtaining the desirable distribution of stresses and displacements along the axis of the specimen (with maximum stress at the centre of the specimen) undergoing ultrasonic fatigue. For this reason, the samples used in this work were designed with threaded extensions in both sides. In the literature this is not always the case. For example, in Drossis' work,⁹ the samples used were designed with a threaded extension in one side and a threaded hole at the other side. Finally, new hardware and software were developed to establish communication between the LCF machine and the HCF power supply, so that various test configurations simulating realistic testing conditions, and not just a simple superposition of LCF and HCF stresses, were possible.

LCF/HCF INTERACTION STUDIES

Experimental set-up

A HCF cell has been designed to operate at 20 kHz. The HCF cell is attached to a servo-hydraulic fatigue machine operating up to 100 Hz. A schematic of the experimental set-up is shown in Fig. 1. An electrical sinusoidal signal of around 20 kHz in frequency is fed to a power amplifier. The amplified electrical signal is converted into mechanical vibrations using two piezoelectric crystals (converter unit). The converter has been specially designed to have a resonance frequency of

20 kHz. The converter also has an air inlet nozzle for cooling air to avoid heating when the unit is used for long durations. The high-frequency and high-amplitude mechanical vibrations are further amplified through a mechanical amplifier (booster horn) and then propagated to the sample. The booster horn has a resonance frequency of 20 kHz. The horn also has a threaded end where the test specimen is attached. As in the case of a cyclic loading device, the above instrument elongates and contracts the sample in the direction of the propagating direction of mechanical vibrations. The rate of elongation and contraction of the sample is at the frequency of the mechanical vibrations. Adjusting the power of the amplifier can control the strain in the sample. An arrangement has been developed to hold the sample and to place the assembly in the grips of a conventional fatigue machine for producing low-cycle fatigue loading. The design of the LCF/HCF system prevents the gripping of the HCF cell from affecting the high-frequency vibrations introduced into the sample. To achieve this, the HCF cell is clamped at the nodal position of the standing wave (negligible longitudinal displacement), which corresponds to the middle area of the mechanical amplifier. The booster horn was designed to have a wider cross-sectional area than at the two ends so it could be clamped to a fixed frame at this point. A second horn (end horn) was designed to be placed on the other end of the specimen. A special set of saddle harnesses was also manufactured to support the horns at their nodal points and allow the entire assembly to be placed in a servo-hydraulic load frame.

To enable HCF/LCF interaction experiments using various testing configurations, the power supply of the HCF cell was connected to the digital controller of the MTS (MTS Systems Corp., MN 55344-2290, USA) fatigue machine (Fig. 2). As shown in Fig. 2, the HCF power supply is connected to the LCF digital controller via a start cable connector, denoted by J6 in the figure. This is a 9-V DSUB male connector in which pin 6 is the +24 V DC source and the pin 2 is the +24 V return. The LCF controller is then connected to a computer via an AT 6450 A/D converter. Special cables were manufactured as follows: the digital output connector of the LCF controller (denoted as DO in the figure) is a 15p DSUB male connector. Pin 1 is DO1 (+), pin 2 is used for the return DO1 RET (–), pin 3 is DO2 (+), and pin 4 is used for the return DO2 RET (–). Similarly, the digital input connector of the LCF controller (denoted as DI in the figure) is a 15p DSUB male connector. Pin 1 is DI1 (+), pin 2 is used for the return DI1 RET (–), and pins 3 and 4 are short circuited.

Software was also developed for the automation of the interaction between the HCF and LCF machines. The

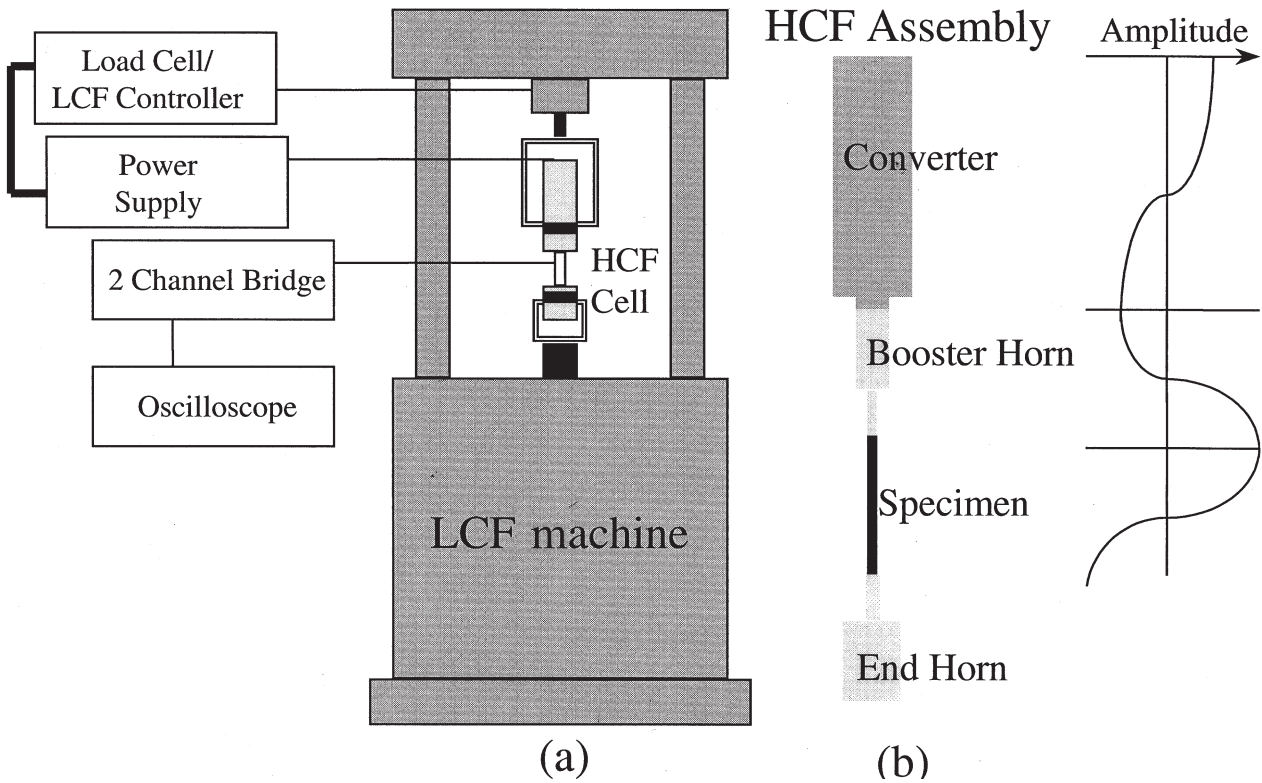


Fig. 1 Schematic of the experimental set-up showing (a) the high-cycle fatigue (HCF) cell placed in a servo-hydraulic low-cycle fatigue (LCD) frame, and (b) the HCF cell assembly.

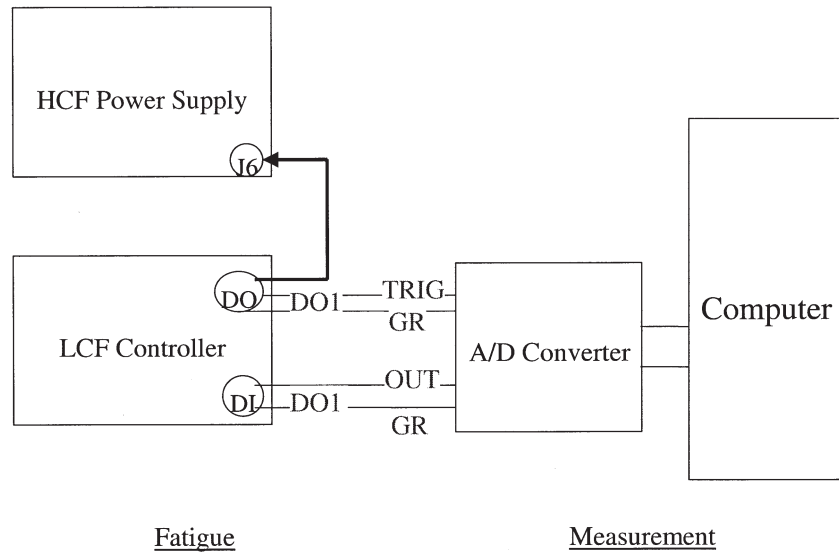


Fig. 2 Hardware developed to enable HCF/LCF interaction experiments using various testing configurations.

schematic of the HCF/LCF interaction procedure is shown in Fig. 3. In this way, various testing configurations are enabled with the new HCF machine. This is a clear advantage in comparison with other existing ultrasonic fatigue machines, which allow only for a simultaneous superposition of LCF and HCF stresses. Next, an example is given illustrating one such testing

configuration. The LCF machine first performs a low cycle, while the HCF power supply remains off, followed by a dwell of certain duration, while the HCF power supply is operating. This dwell represents the mean stress level for the HCF cycles. The whole procedure is repeated (loop) to simulate a realistic HCF/LCF interaction test.

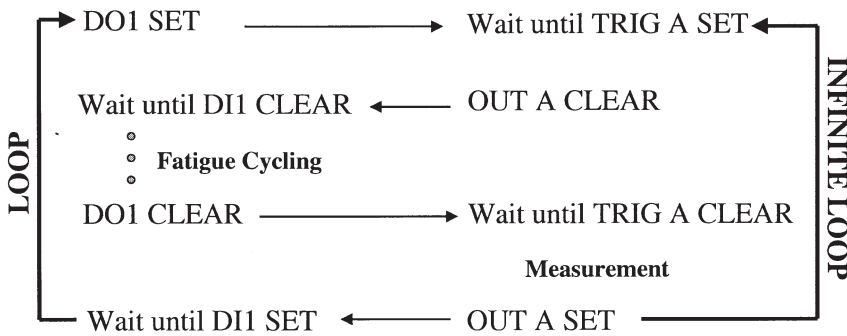
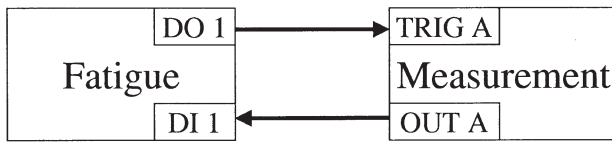


Fig. 3 Automation of ultrasonic fatigue experiments.

Test procedure

To evaluate the newly developed HCF cell operating at 20 kHz, HCF/LCF interaction tests were performed. As, contrary to conventional fatigue testing, there are not yet any testing standards for performing ultrasonic fatigue, it was chosen to use stress levels and testing frequencies similar to those used by Drossis.⁹ In order to compare the results, the LCF trapezoidal wave frequency was kept constant for all tests. This wave consisted of a 0.25 s ramp-up followed by a 5.5 s dwell and a 0.25 s ramp-down, giving an overall cycle period of 6 s, as shown in Fig. 4. This overall cycle will be referred to as the ‘basic unit’ in the following sections of this

paper. During this cycle (basic unit) the HCF load was applied continuously. On two of the tests a triangular waveform was used as the LCF load, consisting of a 0.25 s ramp-up followed by a 0.25 s ramp-down.

As there are not yet any approved standards pertaining to ultrasonic fatigue, the HCF test procedure was developed as familiarity was gained with the equipment. During the fatigue test, the strain was monitored using strain gauges. A strain gauge (Micro Measurements [part of Vishag Measurements Group, Inc, NC 27611, USA] CEA-06-062AQ-350) was fixed directly to the centre of the specimen. This strain gauge is small (4.7 mm–7.7 mm) and has almost zero mass so it does not affect the vibrational characteristics of the system. A second similar

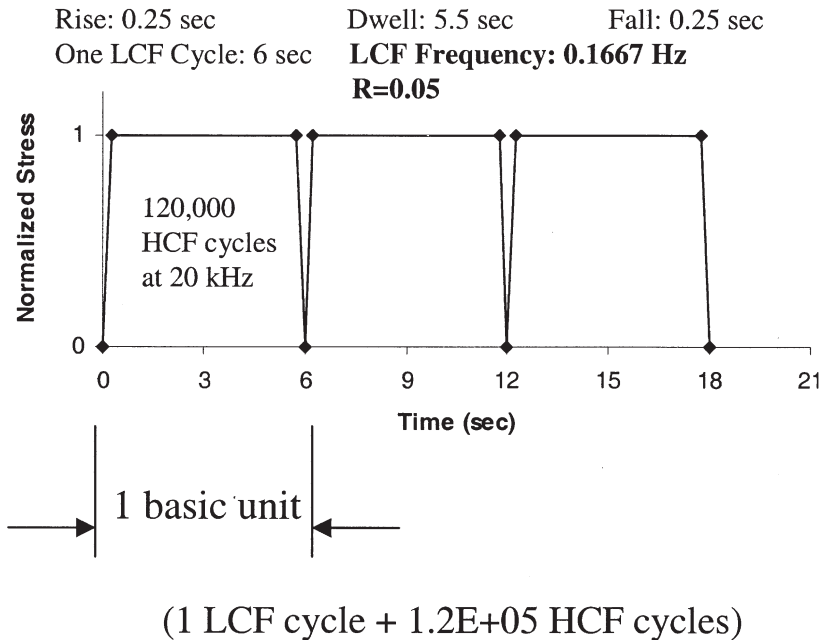


Fig. 4 LCF/HCF test configuration

strain gauge was placed on the end horn. The ratio of the strain measured by the two strain gauges (at the centre of the sample and at the end horn) is constant and depends only on the specimen geometry. A calibration procedure, similar to the one used in Drossis,⁹ was performed for different specimen geometry to determine the strain ratios at the two locations. By using this ratio, only a single strain gauge placed on the end horn is needed for monitoring the strain at the centre of the Ti-6Al-4V specimen. Figure 5 shows the calibration of the strain measurement for two different specimen geometries. One, denoted as type A, had the following geometry: $D1 = 4$ mm, $D3 = 10$ mm, $L1 = 5$ mm, $L2 = 30$ mm, $L3 = 3.15$ mm, resonance length = 76.3 mm (see Fig. 6), the other, denoted as type B, had the following geometry: $D1 = 4$ mm, $D3 = 12$ mm, $L1 = 3$ mm, $L2 = 15$ mm, $L3 = 12.73$ mm, resonance length = 61.46 mm (see Fig. 6). For Ti-6Al-4V, the Young's modulus is $E = 116$ GPa and the yield stress is $\sigma_y = 925$ MPa. The diameter at the gauge section for both specimens was 4 mm. As can be observed from Fig. 5, the ratio $R_e = \epsilon_{\text{specimen}}/\epsilon_{\text{horn}}$ is constant for each specimen geometry. For the specimen of type A, $R_e = 3.6$ and for the specimen of type B, $R_e = 5.2$.

The HCF cell was set up as shown in Fig. 1 complete with the end horn strain gauge connected to a Wheatstone bridge, and the bridge connected to an oscilloscope for monitoring the strain at the end horn. The LCF and HCF loads were then set and the equip-

ment was left running until the test was completed. There are several ways to vary the applied HCF stress on the specimen, by: (i) choosing a specific specimen geometry; (ii) varying the power percentage of the HCF electronics; and (iii) choosing a particular booster horn. For a specimen geometry of type B, when the power is set at 50% and using a booster horn 1:2, the applied HCF stress at the centre of the specimen was around ± 140 MPa. It is estimated that HCF stresses of around 200 MPa could easily be achieved by choosing the appropriate experimental parameters.

An important finding during preliminary ultrasonic fatigue experiments was that the strain at the centre of the specimen could not be maintained constant throughout the test. This means that the ultrasonic fatigue testing was not performed at a constant strain (or at a constant stress). A basic assumption of any meaningful fatigue test is that the experiment is performed at constant strain (or stress). It is therefore important for an ultrasonic fatigue testing system to operate at constant strain or stress, but to achieve this is a major task and most of the existing ultrasonic fatigue machines do not have that capability. In Drossis' work⁹ for example, the nominal stress level is 69 or 138 MPa, however, in the testing procedure this stress level dropped during the test, but was never adjusted during the experiment. There are several reasons for the drop of stress levels during an ultrasonic fatigue experiment. As the fatigue

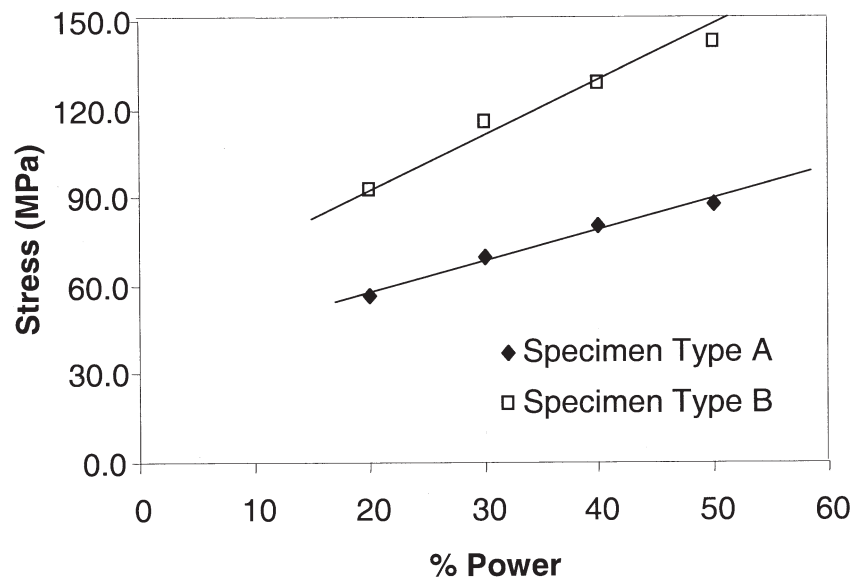
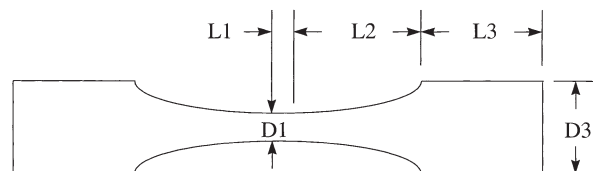


Fig. 5 Strain measurement calibration.

Fig. 6 Longitudinal section of dog-bone-shaped specimen: $L1$, gauge length; $D1$, gauge diameter; $L2$, transition length; $L3$, end length; $D3$, end diameter.



test progresses: (i) elongation of the test coupon occurs, and can be significant especially if a high-stress, low cycle, is superimposed to the ultrasonic fatigue loading. The elongation does not depend on the temperature and the plasticity alone. It also depends on the material behaviour. Titanium alloys elongate more than other materials. (ii) Change in material properties occurs due to substructural changes in the material and fatigue damage accumulation. (iii) A crack may be initiated in the sample and crack growth occurs. The fatigue-related phenomena described above cause a change of the 'effective resonance length' of the test coupon (designed to resonate at a particular frequency—in our case 20 kHz). This change in 'effective resonance length' during the ultrasonic fatigue experiment is a function of sample elongation, substructural changes in the material, and crack growth. A sample with a particular geometry and material property is being designed to have a precise resonance length to resonate at 20 kHz. A change in 'effective resonance length' causes the sample to resonate in a less effective way, i.e. with lower amplitude than in the case of a precise resonance length. Of course, if the resonance length changes significantly, the specimen will not resonate at all. It can be estimated that for such a cut-off in resonance to occur, a difference of more than 10% between the actual and the resonance lengths of the specimen is needed, which is considerably above the changes in 'effective resonance length' observed in ultrasonic fatigue. A lower resonance amplitude means lower strain level at the centre of the sample. To correct for these changes in 'effective resonance length' during ultrasonic fatigue and to maintain the strain (or stress) level during testing, an adjustment of the power level during the test is necessary. This concept contradicts those commonly used in ultrasonic fatigue testing, which is performed at a constant electrical power. The HCF

cell presented here has manually adjusted power level capability. For this reason, the strain adjustment was made manually. It was arbitrarily chosen to adjust the strain twice, consistently for all specimens, during the experiments, at 50 and 100% of the estimated time (or LCF cycles) observed by Drossis.⁹ To manually adjust the strain level, the following procedure was followed. During the test, the steady-state signal from the strain gauge was monitored in the oscilloscope. At 50 and 100% of the estimated time-to-failure of the specimen, the voltage of the electric power supply was manually raised so that the amplitude of the steady-state signal from the strain gauge attains its original value.

Fatigue results

Figure 7 shows the fatigue data from Ti-6Al-4V samples obtained using the HCF cell operating at 20 kHz. A total of 16 samples were tested. For comparison purposes all the specimens were machined from the same stock bar. Different testing conditions were used.

- 1 Three tests were performed with ± 70 MPa HCF stress combined with a LCF stress. The maximum stress for these tests was 725 to 862 MPa. Two of the three tests were run-outs. A run-out of 40 000 low-frequency cycles (or 4.8×10^9 high-frequency cycles) was selected for the tests which included the HCF component. The specimen that did fail had the largest $\Delta\sigma$ of the group and therefore was the one that was expected to fail first.
- 2 Seven tests combined ± 140 MPa HCF stress with a LCF stress. These tests show the severity of the ± 140 MPa high-frequency cycles over that of ± 70 MPa high-frequency cycles, as the fatigue life was reduced by an order of magnitude.

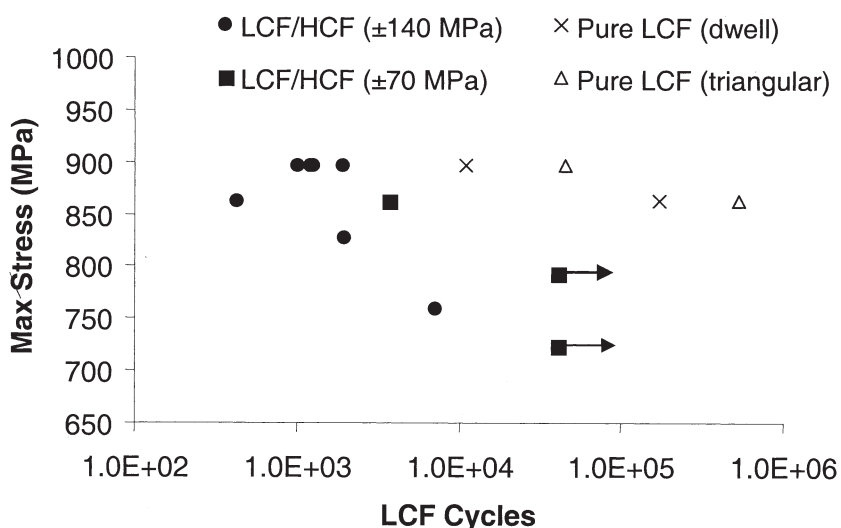


Fig. 7 LCF/HCF testing results using the 20 kHz HCF cell. Results were obtained using the initial parameters of Drossis⁹ and by adjusting the strain level twice, at 50 and 100% of lives.

- 3 For analysis purposes two of the specimens were fatigued at ± 140 MPa HCF stress while they were subjected to a static load. The maximum load and the $\Delta\sigma$ for these tests were the same as in the case of the previous tests that combined HCF with LCF loading.
- 4 Finally, four tests were performed with pure LCF load. In two of them the LCF waveform was trapezoidal (0.25 s rise time and 0.25 s fall time with 5.5 s dwell between the rise and fall of the loading). In the other two the LCF waveform was triangular (0.25 s rise time and 0.25 s fall time). It was observed that eliminating the dwell increased the fatigue life several times.

As has been explained above, the strain level was adjusted twice, at 50 and 100% of the estimated cycles-to-failure observed by Drossis.⁹ The data in Fig. 7 represent the number of cycles-to-failure obtained after the second strain adjustment. When the strain level was adjusted to its initial value, all specimens failed within the same LCF cycle (which has a duration of 6 s). Therefore, the observed lives of the tested specimens were found to be equal to those in Ref. [9]. This means that if the fatigue experiments were performed at constant strain level, the time-to-failure of the specimens would be shorter than the times shown in Fig. 7, where the strain level was not constant. The 'true fatigue life' of the samples is actually between 50 and 100% of the life observed in the experiments. However, given the fact that the HCF cycles-to-failure of the commissioning tests were in the order of 10^7 – 10^8 , the results are a good representation of the order of magnitude of the fatigue life, and therefore, demonstrate that the newly developed ultrasonic fatigue machine provides results that are in agreement with those found in the literature. In fact, the objective of this work was exactly to demonstrate that the HCF cell operates as intended by design, and not to perform a rigorous study of the fatigue life of the particular test coupons.

Analysis

In order to demonstrate that the newly developed apparatus is effective for performing HCF testing, analysis of the data obtained from multilevel cyclic loading was necessary. A cumulative damage analysis was therefore performed to understand more about the fatigue process and determine the relative damage caused by the various fatigue cycle components.

The linear damage rule (LDR)^{9,17,18} proposes that damage caused by multilevel loading can be approximated by summing the ratios of the number of cycles to failure of each of the component cycles of the interactive

load, relative to the number of cycles to failure of each of the component cycles acting individually. The LDR states that damage from each component of the cycle is accumulated linearly, and when the sum of the ratio of component cycles to isolated cycles reaches unity, failure will occur.¹⁸ This is described by the following equation

$$\text{Failure occurs when } \sum \frac{N_i}{N_j} = 1 \quad (1)$$

where N_i is the number of component cycles to failure for interactive load and N_j is the number of cycles to failure for isolated load.

The double linear damage rule (DLDR)^{9,19} also assumes that fatigue damage is linearly additive. However, it goes a step beyond the LDR and separates the damage into two phases: (i) number of cycles until crack initiation, and (ii) number of cycles for crack propagation up to failure. The DLDR is also thought to be more accurate than the LDR. The following relationships are used to determine the theoretical number of cycles or each phase of crack initiation or propagation.

$$\text{Number of basic units for initiation} = \left(\sum \frac{n_i}{N_{fi}} \right)^{-1} \quad (2)$$

$$\text{Number of basic units for propagation} = \left(\sum \frac{n_i}{N_{pi}} \right)^{-1} \quad (3)$$

where

$$N_{fi} = N_{fi} \exp(ZN_f\Phi) \quad (4)$$

$$N_{pi} = N_{fi} [1 - \exp(ZN_f\Phi)] \quad (5)$$

and n_i = number of component cycles per basic unit; N_{fi} = number of cycles to failure for isolated load; Z = experimentally determined constant ($Z = -111.2$ for Ti-6Al-4V); and Φ = experimentally determined constant ($\Phi = -0.523$ for Ti-6Al-4V)

From the above relationships, failure is predicted to occur when the number of interactive load basic units is equal to the sum of the cycles for the crack initiation and the crack propagation phases.

Fatigue tests were performed to isolate the effects of the low-frequency component of the stress cycles. From the results it can be seen that these specimens had significantly higher fatigue lives than the specimens subjected to interactive LCF/HCF loading. Although in some tests the HCF component of the load accounted for only between 15 and 19% of the overall loads, the fatigue lives of these specimens were at least an order of magnitude shorter than the lives of specimens where the HCF component was halved. As can be seen from the results presented in Fig. 7, the HCF component of the

interactive load was responsible for most of the damage causing failure. To illustrate this, the LDR and the DLDR analyses were performed using the test results. The results of these analyses are shown in Figs 8 and 9.

As expected, the results of the DLDR analysis were slightly better (closer to 1) than the LDR analysis for most cases. This is most noticeable as the number of cycles to failure in each of the two single component tests decreases (see Fig. 8). No significant difference between the LDR and DLDR results was observed because of the relatively large number of cycles to failure for these specimens. The large error noted in these analyses indicates that there is a strong interactive effect between the two stress components that the LDR and DLDR do not take into account, as the actual failures occurred 26 to 95% earlier than predicted by both estimations. The LDR analysis did however, confirm the original suspicion that the HCF component of the load was the major contributor to the fatigue failure, as the HCF portions were responsible for between 79.9 and 97.8% of the values obtained according

to the LDR analysis. This observation is illustrated in Fig. 9. The DLDR analysis also highlighted the fact that the majority of cycles (or basic units), between 99.4 and 99.8%, took place in Phase 1 of the crack growth (crack initiation), whereas relatively few cycles were involved in Phase 2 (crack propagation).

HEATING OF THE SPECIMEN DURING ULTRASONIC FATIGUE

During ultrasonic fatigue the specimen is subjected to high-frequency, low-amplitude, vibratory stresses. These vibratory stresses result in heat dissipation. From the distribution of stresses along the axis of the specimen it can be observed that maximum stress levels are present at the centre of the specimen.¹⁶ It is therefore natural to expect that the maximum temperature of the specimen during a HCF test will occur at the centre of the specimen. In order to demonstrate that the newly developed HCF cell is operating properly, this phenomenon

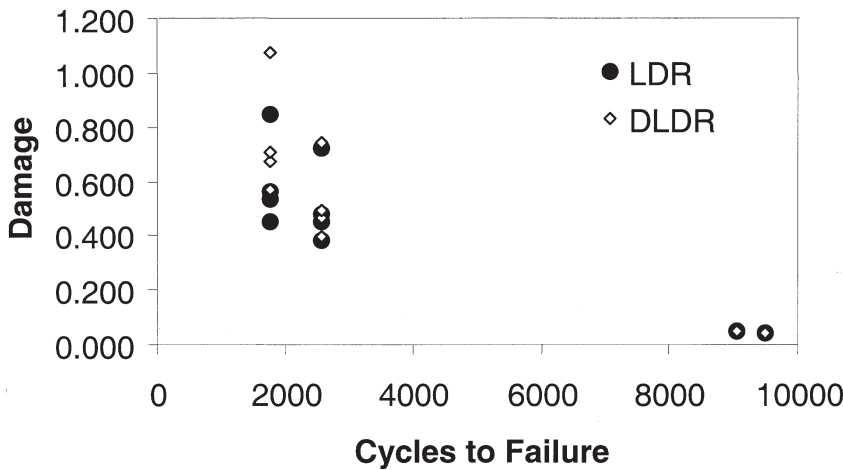


Fig. 8 Linear damage analysis.

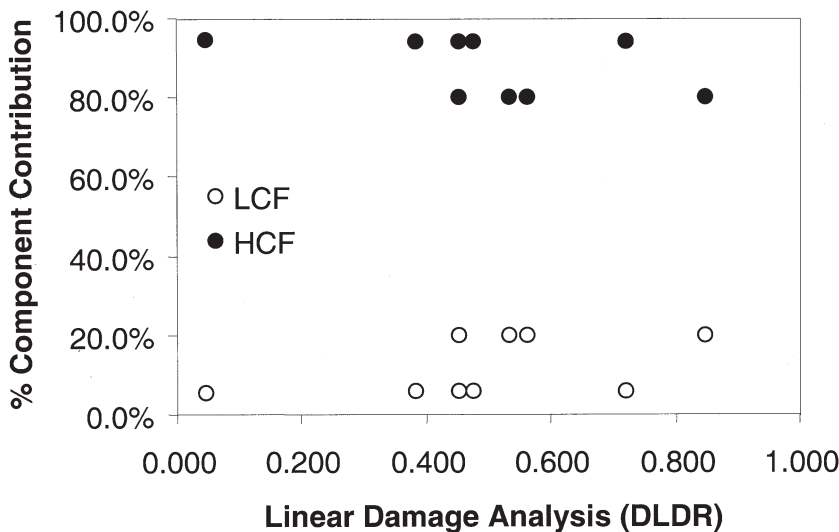


Fig. 9 Contribution of LCF and HCF components to specimen failure.

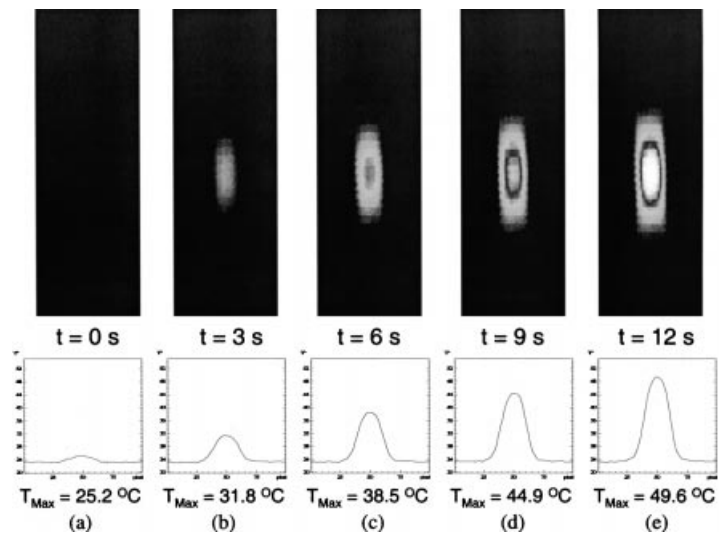


Fig. 10 Heating of a Ti-6Al-4V specimen during high-power ultrasonic loading at 20 kHz.

needs to be verified experimentally. For that reason, the heating of the specimen during HCF has been measured using thermography. An IR camera was used to obtain thermographic images of the specimen *in situ*, during the HCF test, and the surface temperature gradient was calculated. Figure 10 shows the surface temperature distribution during the first 12 s of operation of the HCF apparatus. Figure 10(a) shows that, before the HCF test at $t = 0$, the temperature on the surface of the dog-bone test coupon had a fairly uniform distribution. The initial temperature on the surface of the specimen was 25.2 °C. The temperature on the specimen increased fast as soon as ultrasonic vibratory stresses were applied on the specimen. Figure 10(b)–10(e) demonstrate this. Figure 10(b) shows the thermographic image of the specimen obtained at only 3 s after the start of the HCF test. The surface temperature at the centre of the specimen is now 31.8 °C, which represents a 26% rise in temperature. The heat distribution clearly shows that the maximum temperature occurs at the centre of the specimen. The cross-section plot at the centre of the specimen also demonstrates this. The thermographic images shown in Fig. 10(c) (obtained at 6 s), 10(d) (obtained at 9 s), and 10(e) (obtained at 12 s) show a consistent large increase in temperature during the HCF test with a maximum temperature at the centre of the specimen. The surface temperature at the centre of the specimen at 12 s of operation of the HCF apparatus reached 49.6 °C. The temperature increases in a fairly linear way with time.

SUMMARY

A loading device, capable to fatigue a dog-bone sample at very high frequencies was developed. The fatigue specimens were designed with a particular geometry and resonance length, to obtain the desired levels of strain

and displacement along their length. This ultrasonic fatigue cell can also be attached to a servo-hydraulic LCF machine to provide a second fatigue cycle. The appropriate hardware and software have been developed to interface the HCF cell with the LCF machine enabling interactive LCF/HCF testing to be performed at various loading configurations (different R ratios, $\Delta\sigma_{\text{HCF}}$, $\Delta\sigma_{\text{LCF}}$, etc.). The results obtained in this study using a HCF cell operating at 20 kHz, indicate that the test cell provides a very stable, reliable, and safe method of performing very-high-frequency fatigue tests on a variety of materials. Several LCF/HCF interaction studies were carried out using the HCF cell attached to an MTS LCF fatigue machine and linear damage analysis was used for interpreting the data.

The results of the commissioning test matrix performed on specimens made from a single Ti-6Al-4V bar stock clearly show the effect of the HCF component of the load, in spite of the fact that the HCF component was only 15–19% of the overall load. The results also indicate that the HCF component of the load was the major cause of observed damage with the LCF component having much less effect. Eliminating the HCF component completely resulted in increasing the fatigue life by at least an order of magnitude. This behaviour was also supported by DLDR analysis. The LCF/HCF interactive loading caused failures sooner than predicted by a linear damage law. This indicates that the superimposed loads interact to cause crack growth at a rate, which cannot be modelled by simply comparing the separate components individually. A reason for such an observation could be that the low-frequency load level is instrumental in initiating the crack, whereas the high-frequency load is the main cause of crack growth.

Thermographic monitoring of temperature distribution on the surface of a test coupon during ultrasonic

fatigue demonstrated that there is a significant heating of the specimen during the test and the maximum temperature occurred at the centre of the specimen. This was expected from the analysis.

The fatigue results and analysis demonstrate that the developed ultrasonic fatigue device is indeed inducing HCF damage in the samples. However, a manual adjustment in the strain level during fatigue is not an adequate way to perform reliable HCF testing. An improvement of this system is being currently developed by adding a computerized feedback of the strain level to the HCF power supply, so that the power level can be automatically adjusted to maintain a constant strain level. This automated system will enable the development of a testing capability that: (i) would perform reliable HCF testing, and (ii) could also be used as a non-destructive evaluation (NDE) tool to characterize the material during ultrasonic fatigue and to monitor fatigue crack growth. The variation in the ultrasonic power level as a function of time can be monitored and can be used as an NDE parameter in the above-described concept, as has been shown schematically in Fig. 11. As already explained above, such changes depend on the material properties as well as on the crack growth. Additional analysis will be required to isolate the effect of sample elongation during the test.

Acknowledgements

This work was sponsored by the Defense Advanced Projects Agency (DARPA) Multidisciplinary University Research Initiative (MURI), under Air Force Office of Scientific Research grant number F49620-96-1-0442. The author wishes to express his appreciation to Mr J. Drossis, MURI consultant, for useful discussions, contribution in the selection of components for the ultrasonic fatigue apparatus, help with strain measurements and calibration, and for providing copy of his published work. The author also wishes to thank Dr S. Sathish, University of Dayton, for his help during the construction of the HCF device, Mr G. Blaho for helping with the development of the hardware and software for the automation of the interaction between the HCF and LCF machines, and Mr H. Rösner, Fraunhofer-Institute, Germany, for the use of his IR camera and obtaining the thermographic images.

REFERENCES

- 1 Mason, W. P. (1950) *Piezoelectric Crystals and Their Application in Ultrasonics*. Van Nostrand, New York, USA, p. 161.
- 2 Neppiras, E. A. (1959) Techniques and equipment for fatigue testing at very high frequencies. *Proc. ASTM* **59**, 691–709.

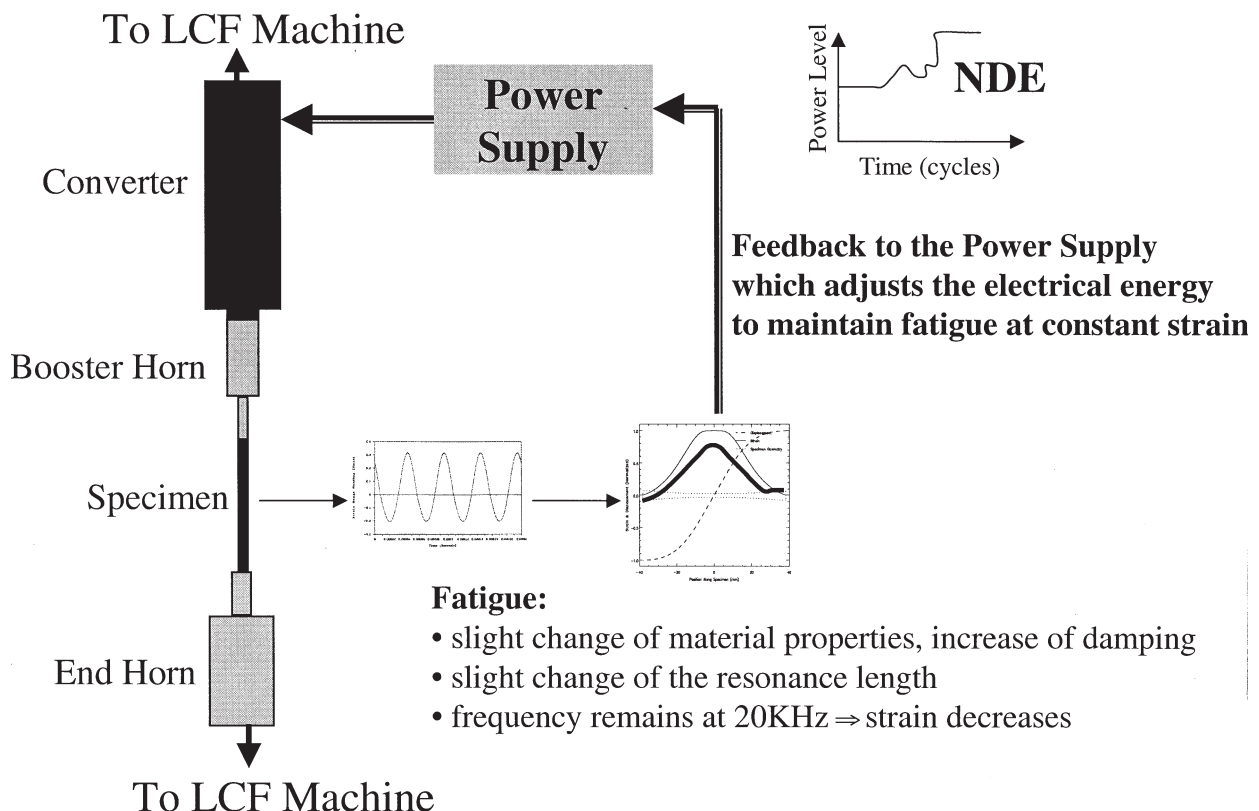


Fig. 11 Automatic adjustment of ultrasonic power and non-destructive evaluation of the damage accumulation during ultrasonic fatigue.

- 3 Eisner, E. and Seager, J. S. (1963) *Safety in Mines Research Establishment*, Report No. 216. HM Stationary Office, London, UK.
- 4 Eisner, E. (1964) *J. Acoust. Soc. Am.* **36**, 309.
- 5 Mason, W. P. and Wick, R. F. (1951) *J. Acoust. Soc. Am.* **23**, 209.
- 6 Hoffelner, W. (1982) *Fatigue of High Temperature Materials at Ultrasonic Frequencies*. Publisher, Town, pp. 645–657.
- 7 Kromp, W., Kromp, K., Bitt, H., Langer, H. and Weiss, B. (1973) Techniques and equipment for ultrasonic fatigue testing. In: *Proceedings of Ultrasonics International Conference*, pp. 238–243.
- 8 Hanson, I. L. H. (1982) Ultrasonic fatigue testing of a rolled valve steel. In: *Ultrasonic Fatigue: Proceedings of the 1st International Conference of Fatigue and Corrosion. Fatigue up to Ultrasonic Frequencies* (Edited by J. Wells). American Institute of Mining/Metallurgical and Petroleum Engineers Inc., Warrendale, PA, USA, pp. 207–217.
- 9 Drossis, J. (1991) The design, development and commissioning of a test facility for HCF/LCF interactive tests. Master's Thesis. University of Toronto, Toronto, Canada.
- 10 Stanzl, S. E., Mayer, H. R. and Tschegg, E. K. (1991) The influence of air humidity on near-threshold fatigue crack growth of 2024-T3 aluminum alloy. *Mater. Sci. Engng* **A147**, 45–54.
- 11 Bathias, C., El Alami, K. and Wu, T. Y. (1997) Influence of mean stress on Ti6Al4V fatigue crack growth at very high frequency. *Engng Fract. Mech.* **56**, 255–264.
- 12 Wu, T. and Bathias, C. (1994) Application of fracture mechanics concepts in ultrasonic fatigue. *Engng Fract. Mech.* **47**, 683–690.
- 13 Xiangnan, K., Saanouni, K. and Bathias, C. (1991) On the fatigue at very high frequency—Part I. theoretical and variational formulation, *J. Engng Mater. Technol.* **113**, 205–209.
- 14 Xiangnan, K., Saanouni, K., Thanigaiyarasu, G. and Bathias, C. (1991) On the fatigue at very high frequency—Part II: application to some materials, *J. Engng Mater. Technol.* **113**, 210–214.
- 15 Anon. (1997) Review on ultrasonic fatigue. In: *ASME Handbook*. ASME, New York, NY, USA.
- 16 Matikas, T. E. (2002) Specimen design for fatigue testing at very high frequencies. *J. Sound Vibrat.* (in press)
- 17 Shoup, T. E. (1984) *Applied Numerical Methods for the Microcomputer*. Prentice Hall, Englewood Cliffs, NJ, USA, pp. 116–123.
- 18 Socie, D. (1983) *Variable Amplitude Fatigue Life Estimation Models*. Society of Automotive Engineers, Warrendale, PA, USA, pp. 2351–2352.
- 19 Manson, S. S. and Halford, G. R. (1981) Practical implementation of the double linear damage rule and damage curve approach for treating cumulative fatigue damage. *Int J. Fracture* **17**, 169–192.